High-throughput competitive fluorescence polarization assay reveals functional redundancy in the S100 protein family

Márton A. Simon[1] [iD], Péter Ecsédi[1], Gábor M. Kovács[2], Ádám L. Póti[3], Attila Reményi[3], József Kardos[1], Gergő Gógl[1,4] [iD] and László Nyitray[1] [iD]

1 Department of Biochemistry, Institute of Biology, ELTE Eötvös Loránd University, Budapest, Hungary
2 Department of Plant Anatomy, Institute of Biology, ELTE Eötvös Loránd University, Budapest, Hungary
3 Institute of Organic Chemistry, Research Center for Natural Sciences, Hungarian Academy of Sciences, Budapest, Hungary
4 Equipe Labellisee Ligue 2015, Department of Integrated Structural Biology, Institut de Genetique et de Biologie Moleculaire et Cellulaire (IGBMC), INSERM U1258, CNRS UMR 7104, Universite de Strasbourg, Illkirch, France

The calcium-binding, vertebrate-specific S100 protein family consists of 20 paralogs in humans (referred as the S100ome), with several clinically important members. To explore their protein–protein interactions (PPIs) quantitatively, we have chosen an unbiased, high-throughput, competitive fluorescence polarization (FP) assay that revealed a partial functional redundancy when the complete S100ome ($n = 20$) was tested against numerous model partners ($n = 13$). Based on their specificity, the S100ome can be grouped into two distinct classes: promiscuous and orphan. In the first group, members bound to several ligands (> 4–5) with comparable high affinity, while in the second one, the paralogs bound only one partner weakly, or no ligand was identified. Our results demonstrate that FP assays are highly suitable for quantitative interaction profiling of selected protein families. Moreover, we provide evidence that PPI-based phenotypic characterization can complement or even exceed the information obtained from the sequence-based phylogenetic analysis of the S100ome, an evolutionary young protein family.

Introduction

Biochemical characterization of protein–protein interactions (PPIs) is a challenging field in molecular life sciences, which is usually limited to the determination of steady-state dissociation constants [1]. The accurate determination of thermodynamic parameters of molecular interactions is performed by fast, but superficial, high-throughput (HTP) methods. In the literature, several HTP approaches are applied such as coimmunoprecipitation [2], yeast two-hybrid and spot assays [3], pull-down assay [4], holdup assay [5], and direct fluorescence polarization/anisotropy [6]. In direct fluorescence polarization (FP) experiments, a fluorescent probe (usually a labeled peptide) is titrated with a globular partner. Their association is monitored by the polarization of the emitted light of the fluorophore (Fig. 1A). In a modified FP experiment called

competitive assay, both the probe and partner concentration are fixed, and the reaction mixture is titrated with an unlabeled competitor molecule (peptide or protein). Depolarization of the emitted light is indicative of the competition between the probe and the competitor in binding to the partner (Fig. 1B,C). While direct FP can be perturbed by the presence of the fluorescent dye, the competitive assay is unbiased and therefore more suitable for accurate HTP measurements of dissociation constants [7,8].

S100 proteins belong to the superfamily of EF-hand containing calcium-binding proteins. They appeared in early vertebrates and consist of 20 core paralogs in the human proteome [9]. S100s are associated with several disease conditions, such as cardiomyopathies, cancer, and inflammatory and neurodegenerative diseases, in which their overexpression can be observed in the affected cells [10–12]. Due to this reason, they are emerging biomarkers and also promising therapeutic targets [13]. Despite their growing importance, the literature still lacks their comprehensive and systematic analysis, which would be essential for developing rational strategies for drug development. Similar to calmodulin, they can interact with protein or peptide targets in a calcium-dependent manner [14]. They are generally considered as relatively low specificity proteins, with dozens of interaction partners, among them they are unable to maintain high selectivity [15]. In this study, we determined the interaction profile of the full human S100 family (termed here as the S100ome)

against a set of diverse known S100 partners (and some of their paralogs) systematically, including kinases such as RSK1 [16] and its paralogs MK2 and MNK1; cytoskeletal elements such as CapZ [17] (commonly known as TRTK12), NMIIA [18], ezrin [19], FOR20 and its paralog FOP [20]; membrane proteins such as NCX1 [15] and TRPM4 [21]; and other signaling proteins such as the tumor suppressor p53 [22–24], SIP [15], and MDM4 [23].

Results

Mapping the S100ome with FP measurements

The interactions between S100 homodimers and their selected labeled peptide partners were studied first by direct FP assay (Figs S1–S13). We have found that all reasonable S100 interactions gave an experimental window of 50–200 mP (polarization). If significant binding was detected ($K_d < 200$ μM) between a labeled peptide and an S100 protein, a subsequent competitive FP assay was performed. In cases, where no labeled peptide was available (e.g., when globular protein domains were used as competitors), we used noncognate tracers against all possible S100 proteins. Additionally, we tested the possible binding between these competitors and the noncognate probes in direct FP experiments to eliminate the possibility of rebinding (Fig. S14). This way, we tested 180 unique direct and 150 unique competitive interactions and found 89 and
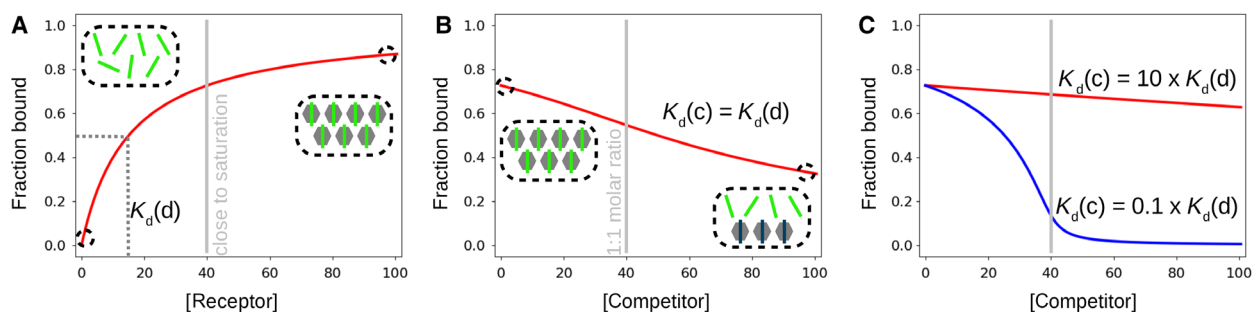
Fig. 1. The theory of fluorescence polarization assays. (A) Fluorescence polarization/anisotropy experiments can be performed with direct and competitive titrations. In direct assay (direct titration, (d)), the concentration of the protein of interest is increased in the presence of tracer amount of labeled peptide. Upon complex formation, the hydrodynamic radius of the tracer increases causing slower rotation and therefore lower depolarization of the emitted light. In the direct assay, one can measure the minimal and maximal polarization values, a dissociation constant, and importantly, an optimal concentration can be easily determined for competitive assays, which is usually the concentration corresponding to 60–80% saturation. (B) In a competitive assay (competitive titration, (c)), the concentration of the protein of interest is set to this concentration and one can titrate the reaction mixture with a competitor. The competition results in increased level of free labeled peptide and consequently high depolarization of the emitted light. (C) Competitive FP is not affected by the presence of a labeling group in the peptide (unbiased) and has a high dynamic range (approximately two orders of magnitudes around the dissociation constant of the probe). At high concentrations, it can be also used to determine the stoichiometry of the interaction for strong interactions. $K_d(d)$ and $K_d(c)$ correspond to direct and competitive dissociation constants, respectively. The red and blue graphs (on panel C) correspond to two scenarios, in which the competitive K_d ($K_d(c)$) is 10-fold higher and 10-fold lower than the direct K_d ($K_d(d)$), respectively.

66 significant interactions, respectively (Table 1, Figs S1–S13).

Compared to the direct assay, competitive FP provides unbiased (or more specific) affinities, unaffected by the chemical labeling, making it a better tool to measure protein–protein interactions (Fig. 2A,B). Nevertheless, there are some pitfalls (Fig. 2), which should be taken into consideration while analyzing competitive data. First of all, the experimental window of the competitive measurement should be the same as the experimental window of the direct measurement (Fig. 2C). Studying large biomolecules (e.g., globular proteins) in a competitive experiment often results in an increased base polarization (P_{min}) due to the change in biophysical properties of the reaction mixture (e.g., change in viscosity). Moreover, during a competition experiment, it is possible that the competitor can interact with the probe itself, which can also cause an increase in the base polarization (Fig. S14). In rare cases, saturation polarization can be also altered (e.g., due to oligomerization at higher concentration). Additionally, experimental artifacts of unknown origin can be observed occasionally (Fig. 2D). Here, a sharp decline can be detected during the titration, which results in an IC50 value smaller than the fixed

Table 1. Quantitative characterization of interactions between S100 proteins and their selected partners by FP (N.D., not determined; E.A., experimental artifact; (d), direct titration; (c), competitive titration).

K_d (µM)											
	fp53 (d)	p53 (c)	fNMIIA (d)	NMIIA (c)	fCapZ (d)	CapZ (c)	fNCX1 (d)	NCX1 (c)	fSIP (d)	SIP (c)	FOR20 (c)
S100A1	41 ± 11	> 200	0.033 ± 0.0062	0.004 ± 0.001	8.9 ± 2.0	5.2 ± 1.7	2.6 ± 0.14	2.6 ± 0.56	> 200	N.D.	0.50 ± 0.25
S100A2	2.9 ± 0.08	5.2 ± 0.39	0.057 ± 0.0038	0.013 ± 0.0022	> 200	N.D.	5.5 ± 0.37	> 200	102 ± 40	> 200	0.27 ± 0.03
S100A3	7.6 ± 0.44	7.7 ± 1.9	5.5 ± 1.0	E.A.	> 200	N.D.	25 ± 2.5	> 200	> 200	> 200	29 ± 5.6
S100A4	0.85 ± 0.04	2.1 ± 0.23	0.026 ± 0.0065	0.0088 ± 0.0025	> 200	N.D.	15 ± 0.62	> 200	42 ± 5.2	11 ± 2.7	2.0 ± 0.20
S100A5	26 ± 2.4	67 ± 23	5.8 ± 0.67	2.9 ± 0.51	4.7 ± 0.28	5.4 ± 0.84	4.6 ± 0.22	5.2 ± 1.1	42 ± 3.2	40 ± 7.8	1.9 ± 0.53
S100A6	0.68 ± 0.020	2.2 ± 0.090	0.58 ± 0.07	0.21 ± 0.04	> 200	N.D.	27 ± 1.8	> 200	8.7 ± 0.48	20 ± 1.1	0.007 ± 0.0018
S100A7	> 200	N.D.	13.1 ± 1.4	E.A.	> 200	N.D.	30 ± 2.1	E.A.	> 200	N.D.	5.9 ± 0.54
S100A8	> 200	N.D.	> 200	N.D.	> 200	N.D.	56 ± 5.0	E.A.	> 200	N.D.	> 200
S100A9	> 200	N.D.	> 200	N.D.	> 200	N.D.	20 ± 3.2	> 200	> 200	N.D.	> 200
S100A10	48 ± 2.9	> 200	> 200	N.D.	> 200	N.D.	53 ± 6.6	> 200	> 200	N.D.	> 200
S100A11	10 ± 0.72	12 ± 2.4	49 ± 14	E.A.	> 200	N.D.	52 ± 2.9	E.A.	> 200	N.D.	> 200
S100A12	76 ± 11	N.D.	> 200	N.D.	> 200	N.D.	170 ± 63	E.A.	> 200	N.D.	> 200
S100A13	35 ± 10	> 200	> 200	N.D.	> 200	N.D.	87 ± 14	E.A.	> 200	N.D.	> 200
S100A14	> 200	N.D.	98 ± 127	E.A.	> 200	N.D.	71 ± 7.5	E.A.	> 200	N.D.	63 ± 30
S100A15	> 200	N.D.	17 ± 1.5	E.A.	> 200	N.D.	28 ± 3.4	E.A.	> 200	N.D.	17 ± 2.1
S100A16	79 ± 8.9	N.D.	> 200	N.D.	> 200	N.D.	> 200	N.D.	> 200	N.D.	> 200
S100B	33 ± 3.2	> 200	4.7 ± 0.25	2.9 ± 0.31	2.3 ± 0.13	1.8 ± 0.23	7.7 ± 0.95	> 200	> 200	N.D.	0.25 ± 0.050
S100G	> 200	N.D.	21 ± 1.9	E.A.	> 200	N.D.	24 ± 1.7	E.A.	> 200	N.D.	3.8 ± 1.1
S100P	0.17 ± 0.01	0.54 ± 0.040	0.99 ± 0.11	0.14 ± 0.03	11 ± 1.4	4.1 ± 0.73	4.0 ± 0.23	> 200	38 ± 3.2	> 200	1.2 ± 0.13
S100Z	> 200	N.D.	> 200	N.D.	> 200	N.D.	11 ± 0.45	E.A.	> 200	N.D.	> 200

K_d (µM)											
	fTRPM4 (d)	TRPM4 (c)	fMDM4 (d)	MDM4 (c)	fC-ERMAD (d)	C-ERMAD (c)	fRSK1 (d)	RSK1-CTKD (c)	MK2 (c)	MNK1 (c)	FOP (c)
S100A1	0.38 ± 0.061	> 200	91 ± 14	35 ± 10	> 200	N.D.	4.8 ± 0.72	> 200	15 ± 4.6	> 200	0.35 ± 0.14
S100A2	1.0 ± 0.062	1.1 ± 0.23	49 ± 10	53 ± 16	15 ± 0.62	5.4 ± 0.57	5.1 ± 0.53	> 200	4.5 ± 1.0	18 ± 4.2	0.081 ± 0.019
S100A3	0.91 ± 0.052	3.4 ± 0.45	> 200	N.D.	> 200	N.D.	> 200	N.D.	> 200	> 200	0.27 ± 0.13
S100A4	5.9 ± 0.36	35 ± 113	> 200	N.D.	11 ± 0.73	6.1 ± 0.80	8.5 ± 0.89	> 200	> 200	24 ± 3.5	0.048 ± 0.010
S100A5	0.60 ± 0.051	2.3 ± 0.71	61 ± 5.4	65 ± 7.5	> 200	N.D.	> 200	N.D.	> 200	> 200	0.56 ± 0.20
S100A6	1.4 ± 0.081	8.4 ± 2.0	> 200	N.D.	> 200	N.D.	8.7 ± 0.81	> 200	> 200	6.7 ± 0.53	0.0056 ± 0.0050
S100A7	> 200	N.D.	> 200	N.D.	> 200	N.D.	> 200	N.D.	E.A.	E.A.	> 200
S100A8	3.8 ± 0.57	13 ± 4.4	> 200	N.D.	> 200	N.D.	> 200	N.D.	N.D.	> 200	> 200
S100A9	21 ± 7.3	> 200	> 200	N.D.	> 200	N.D.	> 200	N.D.	N.D.	> 200	> 200
S100A10	17 ± 1.9	125 ± 25	> 200	N.D.	> 200	N.D.	> 200	N.D.	> 200	> 200	> 200
S100A11	2.4 ± 0.12	106 ± 11	> 200	N.D.	> 200	N.D.	> 200	N.D.	> 200	> 200	> 200
S100A12	> 200	N.D.	> 200	N.D.	> 200	N.D.	> 200	N.D.	N.D.	> 200	> 200
S100A13	> 200	N.D.	> 200	N.D.	> 200	N.D.	> 200	N.D.	N.D.	N.D.	> 200
S100A14	12 ± 5.6	> 200	> 200	N.D.	> 200	N.D.	> 200	N.D.	E.A.	E.A.	> 200
S100A15	> 200	N.D.	> 200	N.D.	> 200	N.D.	> 200	N.D.	E.A.	E.A.	> 200
S100A16	> 200	N.D.	> 200	N.D.	> 200	N.D.	> 200	N.D.	N.D.	> 200	> 200
S100B	16 ± 25	> 200	0.20 ± 0.04	0.15 ± 0.04	> 200	N.D.	2.8 ± 0.47	1.2 ± 0.86	3.2 ± 0.73	1.2 ± 0.53
S100G	> 200	N.D.	> 200	N.D.	> 200	N.D.	> 200	N.D.	E.A.	E.A.	> 200
S100P	0.93 ± 0.24	> 200	> 200	N.D.	> 200	N.D.	4.5 ± 0.47	> 200	2.7 ± 0.47	2.5 ± 0.38	0.066 ± 0.0049
S100Z	> 200	N.D.	> 200	N.D.	> 200	N.D.	> 200	N.D.	N.D.	N.D.	> 200
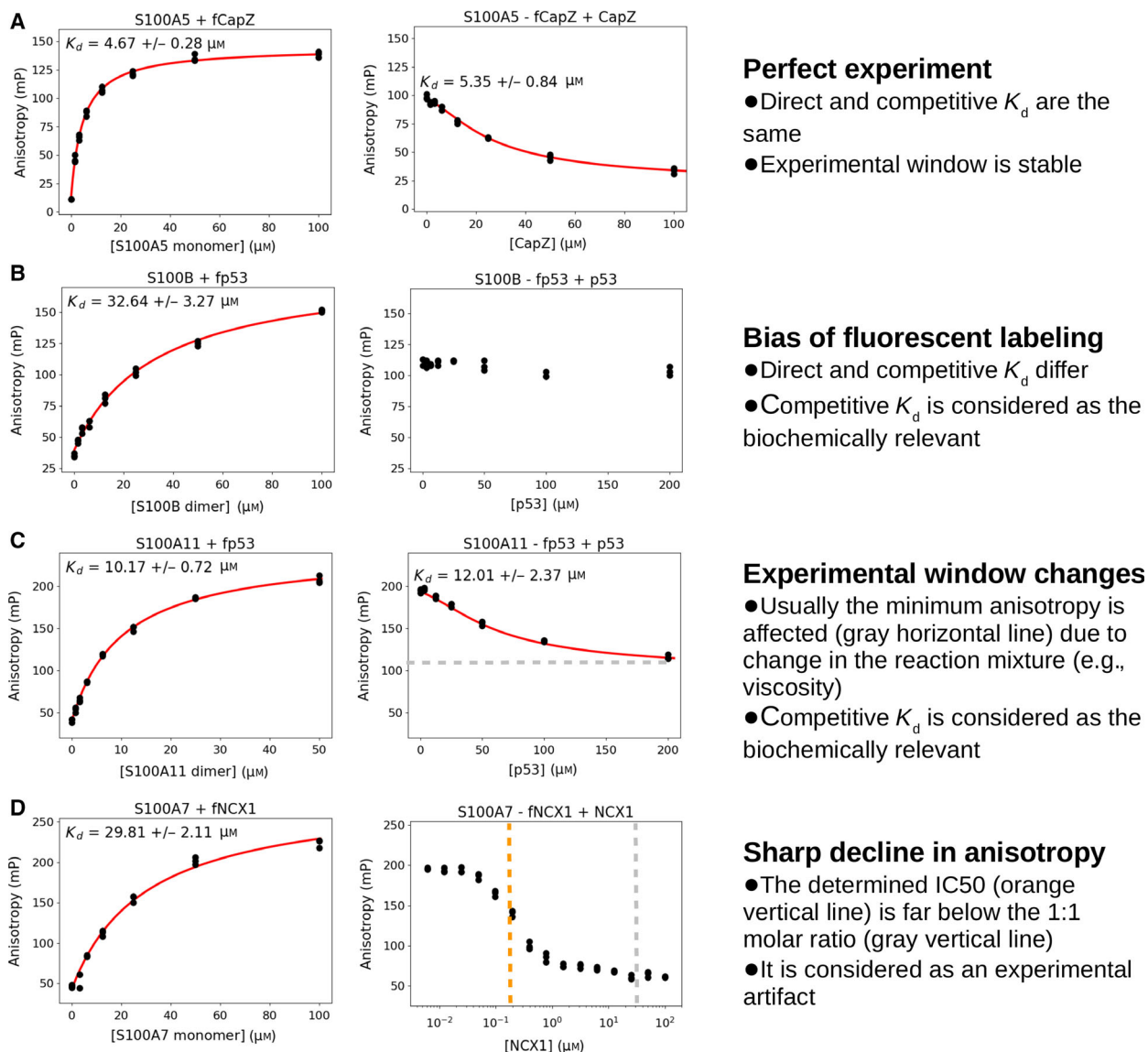
Fig. 2. Possible outcomes of a competitive experiment. (A) In 'perfect experiments', the experimental window is stable and the dissociation constants match between the (cognate) probe and the competitor. (B) As often occurs, fluorescent labeling can alter the binding affinity, resulting in false-positive interaction partners in direct FP experiments. In other cases, the effect is softer and it only causes a dimming effect on the biochemical constant. (C) The reliable experimental window can be different in a competitive experiment. If the change is not extreme, the competitive K_d can be considered (with caution) as the relevant biochemical constant. (D) In some cases, a rapid decline can be observed in the polarization. In this case, the experimentally determined IC50 value should not be used as a dissociation constant. This phenomenon can be explained by a competitor-induced biophysical transition, for example, aggregation or precipitation. In this final case, it is very important to redetermine the concentrations of the receptor and the competitor and to repeat the experiment at different receptor concentrations to properly discriminate the stoichiometric molar ratio from the observed IC50 value.

receptor concentration. This observed substoichiometric complex formation should be handled with extra care as it is likely due to unexpected biophysical phenomena, such as protein aggregation. To standardize and automatize data handling and to eliminate subjective factors, we developed a Python-based universal program, called ProFit, for fitting all direct and competitive experimental data (freely available at https://github.com/GoglG/ProFit).

Validation with ITC measurements

The biochemically described S100 binding motifs, found in the literature, show an extremely low

sequence similarity [15,23] (Fig. 3A). Mostly, linear segments are recognized by the human S100ome; however, no consensus S100 binding sequence can be defined [15]. In general, hydrophobic residues are preferred, but additional basic residues can also be favored in some instances. Moreover, S100 proteins can form two types of complexes (Fig. 3B). Earlier studies showed that a symmetric S100 dimer can recognize two identical binding motifs (1 S100 dimer binds 2 partners, $N = 1$), symmetrically [17,25,26]. In recent studies, however, several asymmetric complexes (1 S100 dimer binds 1 partner, $N = 0.5$) were also described [18,27,28]. In those cases, an S100 dimer captures a single partner at the two binding sites. As the binding affinity highly depends on the stoichiometry of the interaction, we selected a set of significant, peptide-based interactions for isothermal titration calorimetric (ITC) measurements. This way, we validated the interactions that were originally detected by the FP assay and determined the binding stoichiometry in all instances.

All determined K_d values correlated well with the data provided by the orthogonal FP measurements (Table 2, Fig. S15). Symmetric interactions were found with CapZ, NCX1, SIP, TRPM4, and MDM4. In cases of CapZ and MDM4, the experimental data were fitted by a two binding site model indicating slightly different affinities and a complex relationship between the S100 monomers. In contrast, asymmetrical interactions were detected with p53, RSK1, C-ERMAD, NMIIA, and FOP. These findings confirmed the expected binding stoichiometry in all cases and clarified the binding mode of TRPM4 and FOP. We hypothesize that the binding mode of close paralogs should be identical (symmetric or asymmetric); therefore, asymmetric binding was assumed for MNK1,

MK2 (based on RSK1), and FOR20 (based on FOP). We performed these ITC measurements in parallel with the FP experiments, and based on the refined stoichiometry, monomer or dimer S100 concentrations were used during the FP data evaluation.

Specificity map of the S100ome

The 20 S100 paralogs, whose interactions were studied here, represent almost the complete human S100ome [13]. It is a chordata-specific, evolutionary young protein family, and despite the fact that they exhibit moderate sequence similarity, they are structurally very similar owing to their small size (~ 100 residues) and conserved fold (including two consecutive EF-hand motifs) (Fig. 4A). Due to this reason, their phylogenetic analysis generally does not lead to unambiguous results [29,30]. Applying different parameters during the analyses resulted in varied grouping of the human S100ome; moreover, only a few clades received statistical supports (see our analyses in Fig. 4B). Because of these ambiguities of the phylogenetic analyses, a phenotypic screening and analysis could provide a more reliable grouping and could reveal functional similarities among the paralogs of the protein family of interest beside the sequence-based genealogies. For such purpose, we decided to create a robust phenogram [31], representing the functional relationships within the human S100ome, using hierarchical clustering (UPGMA) [32]. This analysis separated the S100ome into two groups, in which the first group contains S100 proteins generally lacking significant interactions (termed here as 'orphan' S100 proteins) and the second group comprises generally good binders (termed here as 'promiscuous' S100 proteins) (Fig. 5). While promiscuous S100 proteins showed significant binding
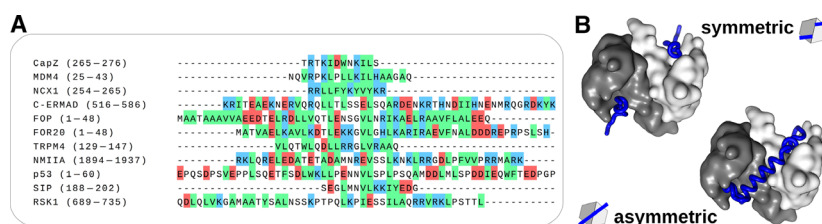
Fig. 3. The S100 protein family. (A) Multiple short linear motifs are recognized by S100 family members; however, no consensus-binding motif can be defined for the protein family, as indicated here by the sequence alignment of several S100 binding motifs by ClustalW algorithm (UniProt accession codes: CapZ: P52907, MDM4: O15151, NCX1: P32418, C-ERMAD: P15311, FOP: O95684, FOR20: Q96NB1, TRPM4: Q8TD43, NMIIA: P35579, p53: P04637, SIP: Q9HB71, RSK1: Q15418). Though it is noteworthy that hydrophobic residues (green) are preferred, basic residues are also welcome in some cases. (B) S100 proteins act as dimers and are capable of interacting in two distinct ways with other proteins. On the left, a symmetric complex is shown, where one S100 dimer interacts with two peptides (S100B-CapZ, PDB code: 1MWN, [17]). By contrast, a single interacting partner can bind to one S100 dimer asymmetrically, as it is shown on the right side (S100A4-NMIIA, PDB code: 3ZWH, [18]). PYMOL (Schrödinger, New York, NY, USA) was used for visualization and for preparing molecular images.

Table 2. Quantitative characterization of interactions between S100 proteins and their selected partners by ITC.

Measurement	T (K)	N (mol peptide·mol^{-1} S100 subunit)	Reference N (mol peptide·mol^{-1} S100 subunit)	K_d (μM)	ΔH (kJ·mol^{-1})	$-T\Delta S$ (kJ·mol^{-1})
S100A6-FOP	310	0.44 ± 0.002	Previously unknown	0.088 ± 0.0073	−73 ± 0.58	31
S100B-CapZ	310	0.44 ± 0.002	1 [17]	3.9 ± 0.39	−15 ± 0.37	−17
		0.343 ± 0.002		0.94 ± 0.03	−3.3 ± 0.67	−33
S100A1-NCX1	310	1.1 ± 0.013	1 [15][a]	6.4 ± 0.58	−35 ± 0.80	4.0
S100A5-TRPM4	310	0.89 ± 0.0037	Previously unknown	1.4 ± 0.089	−24 ± 0.21	−10
C-ERMAD-S100A4	310	0.52 ± 0.015	0.47 [19]	18 ± 2.7	−49 ± 3.0	22
S100A5-SIP	310	0.92 ± 0.24	1 [26][a]	21 ± 20	−4.1 ± 2.5	−24
S100A1-NMIIA	298	0.49 ± 0.0017	0.5 [18][a]	0.009 ± 0.005	36 ± 0.34	−82
S100B-MDM4	310	0.52 ± 0.039	1 [23]	0.71 ± 0.036	−186 ± 142	150
		0.53 ± 0.038		0.63 ± 0.081	111 ± 148	−148

[a] These interactions were measured with a different S100 paralog.

to at least a few (4–5) of the tested interaction partners, orphan S100 proteins showed either no sign of partner binding or a weak binding to a single partner.

Discussion

Competitive FP as a potent tool to measure high-throughput macromolecular interactions

Although numerous HTP, semiquantitative approaches are available and many low-throughput but highly accurate methods exist to measure PPIs, reliable and quantitative HTP methods are scarce in the literature. On the one hand, direct FP assay can be performed in large scale in multiwell plates, which makes it an ideal method for rapid interaction screening; however, it has the serious limitation of chemical labeling that can perturb the binding measurement. Competitive FP, on the other hand, shares the same properties but without any possible interference from the labeling dye. Moreover, it provides comparative results to other, orthogonal, usually low-throughput, label-free biochemical assays, such as ITC or SPR measurements [33]. In the present work, we applied this robust HTP method to characterize the specificity map of the S100 interactome. We used minimal S100 binding segments (with a few exceptions) due to technical and biochemical reasons. On the one hand, this is a limitation, because the presented affinities might be different in full-length proteins, but on the other hand, the generated data set remained as comparative as possible between different S100 proteins. One should note that binding stoichiometry and oligomerization of the investigate proteins, in this case, S100s, could affect the FP measurements and data evaluation. As both properties could affect the binding ratio and the affinity,

orthogonal measurements are important as part of the validation process [34]. In summary, competitive FP assay is robust and has HTP; thus, it is a valuable tool for screening macromolecular interactions involving linear peptide motifs, RNA/DNA oligonucleotides, or fluorescent small molecules [35,36].

Functional redundancy within the S100 family and possible functions of the orphan group

S100 proteins are usually considered as 'sticky', relatively low specificity proteins [15], which is also supported by several studies covering nearly all S100 proteins and only one or few S100 targets [20,37–41]. Usually, the tested S100 proteins only covered the closest relatives (e.g., S100A2, S100A4, S100A6, S100B, S100P), and the results often showed redundant bindings [19,27,40,42,43]. In one study, close to the full S100ome was tested against a simple peptide (derived from CapZ), highlighting binding promiscuity for a subset of S100 isoforms [38]. However, no systematic study has been performed to make a specificity map involving the complete S100ome against multiple S100 partners. Based on functional clustering, we have revealed here that the S100ome can be separated into two groups, which is comparable with previous findings based on few partners. The minor group of eight members includes promiscuous paralogs, which clearly suggests functional redundancy, at least *in vitro*. However, this does not mean that they do not have specific interactions (e.g., RSK1 is highly specific partner of S100B) In contrast, the major group consists of 12 members without a clear binding preference. The function of this orphan group on the molecular level is less defined. All the dimeric S100 proteins (with the exception of S100A10) are calcium sensors; however, if they
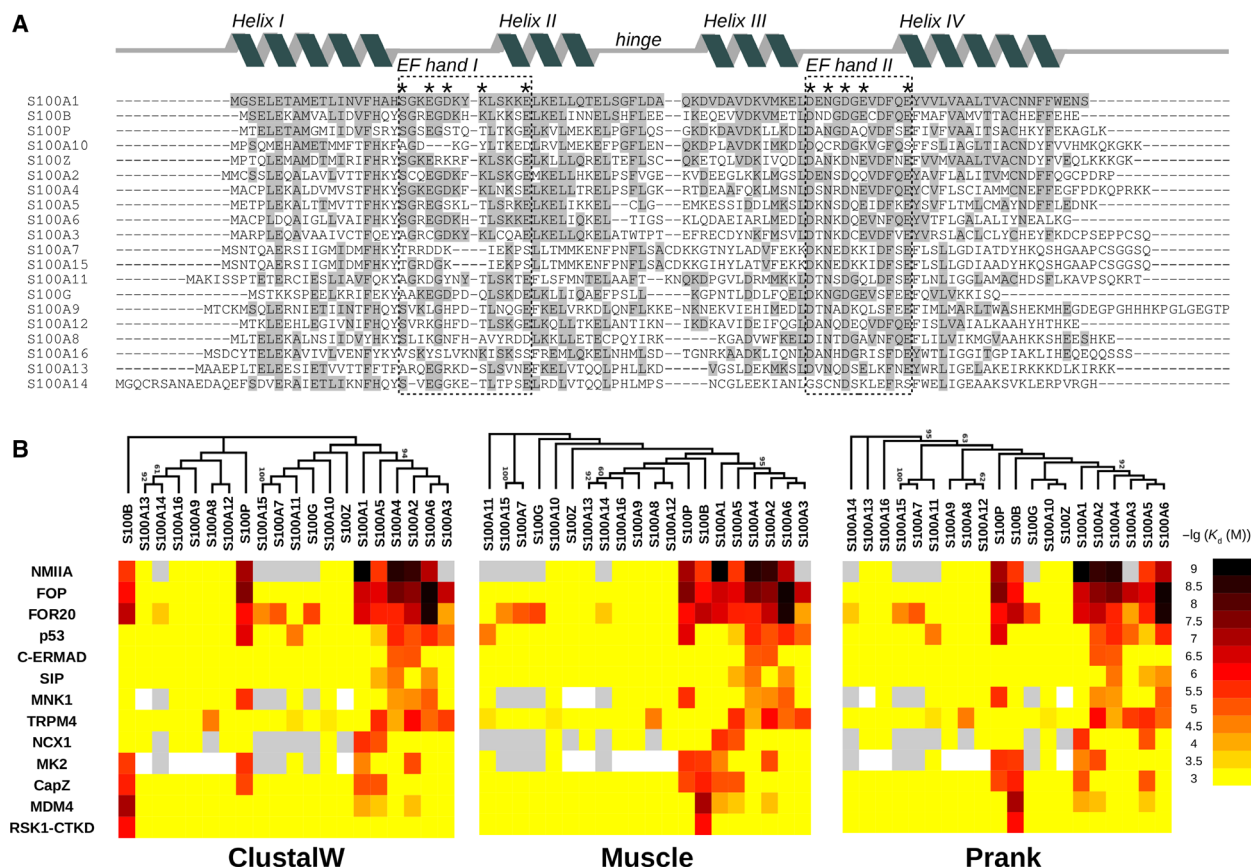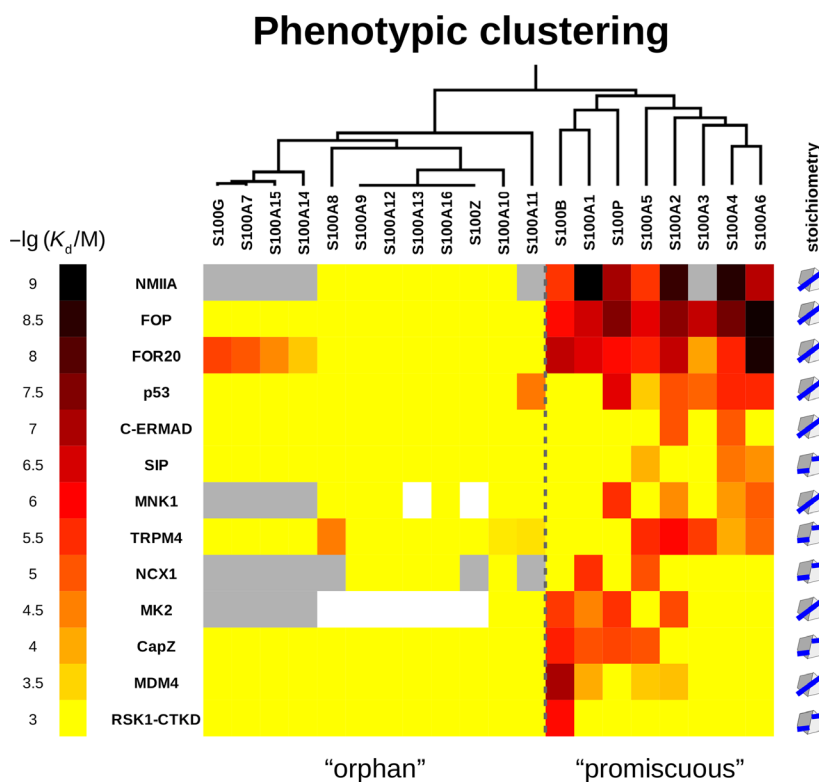
Fig. 4. Phylogenetic map of the S100 protein family. (A) S100 proteins are small (~ 100 amino acids long) EF-hand proteins, sharing high sequence identity (identical residues with S100A1 are shown in gray). The sequences were aligned by CLUSTALW algorithm (UniProt accession codes: S100A1: P23297, S100A2: P29034, S100A3: P33764, S100A4: P26447, S100A5: P33763, S100A6: P06703, S100A7: P31151, S100A8: P05109, S100A9: P06702, S100A10: P60903, S100A11: P31949, S100A12: P80511, S100A13: Q99584, S100A14: Q9HCY8, S100A15: Q86SG5, S100A16: Q96FQ6, S100B: P04271, S100G: P29377, S100P: P25815, and S100Z: Q8WXG8). The fold consists of two consecutive EF-hand motifs, connected by a hinge region. The calcium ions are coordinated by several residues between helices I–II and III–IV (- highlighted with asterisks). (B) The affinity profile of S100ome is clustered by the phylogeny of the different S100 paralogs. For the phylogenetic analyses, the human S100 paralog sequences were aligned by CLUSTALW, MUSCLE, and PRANK algorithms with default parameters (see Materials and methods section). The evolutionary histories were inferred by maximum-likelihood method with 10 runs, using ProtGamma and LG as substitution model and substitution matrix, respectively. The supports of the branches were tested by bootstrap analysis (1000 replicates) shown as % (values below 60% are not shown). The analyses were conducted by RAXML GUI. It is shown that S100A2/A3/A4/A5/A6 and S100A13/A14 can be considered as monophyletic groups, supported by high values (S100A7/A15 are almost identical paralogs). Nevertheless, the phylogenetic analyses do not provide unambiguous genealogy for the rest of the S100 proteins.

have no additional interaction partners, which is difficult to prove, they could simply act as calcium buffers (like S100Z) contributing to calcium homeostasis of the cells [44]. Alternatively, and more likely, they can have highly specific, yet undiscovered, interaction partners. In this case, the orphan designation is only temporary and reflects a limitation of our analysis. For example, S100A10, the only S100 protein without a functional EF-hand motif, can mediate a very high affinity and rather specific interaction with annexin A2 [42]. It is still possible that there is functional redundancy within the orphan group, but our knowledge

about S100 interaction partners is more limited in this group compared to the promiscuous group as no known interaction partners are available. Moreover, the present study covered only S100 homodimers (and the S100G monomer), although some S100 proteins can form heterodimers [45]. As an example, the S100A8/A9 (both coming from the orphan group) can form a functional heterodimer with known interaction partners [46].

Based on an interaction specificity map of the S100 proteins, we propose here that a more widespread functional redundancy exists in the family than

Phenotypic clustering

Fig. 5. The phenogenetic map of the S100 protein family. The determined dissociation constants are depicted as a heatmap representing the specificity map of the S100ome. Hierarchical clustering, based on functional relationships, divided the S100ome into two different groups, one of them consists of low(er) specificity and/or more promiscuous S100 proteins ('promiscuous'), while the other one contains high(er) specificity and/or less promiscuous members of the family ('orphan'). White and gray fields indicate nondetermined interactions and cases with experimental artifacts, respectively. Stoichiometry (2 mol peptides/2 mol S100 subunit, $N = 1$; 1 mol peptides/2 mol S100 subunit, $N = 0.5$) is also shown for all ligands at the end of each rows.

previously thought. Our results provide thermodynamic evidence for possible complex formation with minimal binding segments, and further studies are needed to see whether individual complexes can be indeed formed in a particular cell type and to test that functional redundancy also exists *in vivo*. Regarding the possible biological relevance, the hereby defined functional redundancy can act as a potential compensatory mechanism under pathological conditions, in which the expression patterns and levels of multiple S100 proteins are altered [12].

Function-based examination of relationships within the S100ome complements phylogenetic analysis

The phylogenetic analyses of the human S100ome resulted in rather ambiguous genealogies, likely due to the young age of the protein family (Fig. 4B). Nevertheless, the clade including S100A2, S100A3, S100A4, S100A5, and S100A6 was supported with high statistical values in all analyses (Fig. 4B) similarly as it had also been found by others [29,30]. Our functional analysis has revealed that all members of this clade belong to the same subset of the promiscuous group, with a greatly similar functional profile. However, the phylogeny of the rest of the S100ome is supported with

lower statistical values. Therefore, we suggest that in such scenarios, function-based phenotypic clustering can complement or even exceed the information obtained from pure sequence-based phylogenetic analysis [47]. In our case, the S100 family can be divided, relatively unambiguously, into two bigger clusters (Fig. 5), thus giving a more robust classification. Mapping the specificity and clustering of the S100ome contribute to the better understanding of this vertebrate-specific Ca2+-binding protein family. An implication of the functional redundancy defined hereby is a possibility that a function-based combinatorial theranostic strategy may be more effective than detecting individual proteins of the S100 family.

Materials and methods

Expression and purification of S100 proteins

Protein preparations were done as described previously [48]. Briefly, the cDNAs of S100 proteins were cloned into a modified pET15b expression vector. All protein constructs were expressed in *Escherichia coli* BL21 (DE3) cells (Novagen, Kenilworth, NJ, USA) with a tobacco etch virus (TEV)-cleavable N-terminal His$_6$-tag, and purified by Ni^{2+} affinity chromatography. The His$_6$-tag was cleaved by TEV protease, which was followed by either hydrophobic

interaction chromatography, ion-exchange chromatography, or size-exclusion chromatography with applying standard conditions [48]. The quality of the recombinant proteins was checked by SDS/PAGE analysis.

Expression and purification of kinases

The kinase domains, RSK1-CTKD (411–735), MK2 (1–400), and MNK1 (1–465), were cloned into a variant pGEX expression vector. The kinase domains were expressed in *E. coli* ROSETTA (DE3) cells (Novagen) with TEV-cleavable N-terminal GST and a noncleavable C-terminal His$_6$-tag. The recombinant proteins were purified using Ni^{2+} and GST affinity purification. The quality of the kinase domains was checked by SDS/PAGE analysis. FP measurements were performed without cleavage of the GST-tag.

Expression and purification of recombinant peptides

The peptides FOR20 (1–48), FOP (1–48), p53 (1–60; 17–53), NMIIA (1894–1937), C-ERMAD (516–560 and 516–586), and RSK1 (696–735 and 689–735) were expressed in *E. coli* BL21 (DE3) cells (Novagen) with TEV-cleavable N-terminal GST-tag, and purified by GST affinity chromatography. The tag was cleaved by TEV protease. After cleavage, the TEV protease and GST-tag were eliminated by heat denaturation and centrifugation. The supernatant was purified by RP-HPLC using a Jupiter 300 Å C$_5$ column (Phenomenex, Torrance, CA, USA). The quality of the expressed peptides was checked by mass spectrometry (Bruker Daltonics, Billerica, MA, USA).

Peptide synthesis

The CapZ (265–276), NCX1 (254–265), SIP (188–202), TRPM4 (129–147), and MDM4 (25–43) peptides were chemically synthesized using solid-phase peptide synthesis with a PS3 peptide synthesizer (Protein Technologies, Tucson, AZ, USA) with Fmoc/*t*Bu strategy in the case of 5(6)-carboxyfluorescein-labeled and 5(6)-carboxyfluorescein-unlabeled version. Peptides were purified by RP-HPLC using a Jupiter 300 Å C$_{18}$ column (Phenomenex). The quality of the peptides was monitored by HPLC-MS (Agilent, Santa Clara, CA, USA).

Determination of concentrations

Concentrations of peptides and proteins were determined by UV spectrophotometry using the absorbance of Tyr and Trp residues. In the absence of these aromatic residues, the concentrations were calculated by using the absorbance of the compound on 205 and 214 nm [49,50].

Fluorescent labeling

Chemically synthesized peptides (CapZ, NCX1, SIP, TRPM4, and MDM4) were labeled with 5(6)-carboxyfluorescein (Sigma-Aldrich, St. Louis, MO, USA) at the N terminus at the end of the synthesis. The recombinant peptides (p53, NMIIA, and RSK1) were labeled with fluorescein isothiocyanate (Sigma-Aldrich) at an N-terminal Cys residue using the protocol described previously [48]. C-ERMAD was labeled by Alexa Fluor 568 C$_5$ maleimide (Molecular Probes, Eugene, OR, USA) [19]. The excess labeling agent was eliminated by using HiTrap Desalting column (GE Healthcare, Little Chalfont, UK). The labeled peptides were further purified and separated from the unlabeled peptides by RP-HPLC using a Jupiter 300 Å C$_5$ column (Phenomenex). The concentration of fluorescent peptides and the efficiency of labeling were determined by measuring the absorbance of the fluorescent dye and the peptides.

FP measurements

Fluorescence polarization was measured with a Synergy H4 plate reader (BioTek Instruments, Winooski, VT, USA) by using 485 ± 20 nm and 528 ± 20 nm, and 530 ± 25 nm and 590 ± 35 nm band-pass filters (for excitation and emission, respectively) in cases of fluorescein-based (former) and Alexa Fluor 568-based (latter) measurements. In direct FP measurements, a dilution series of the S100 protein was prepared in 96-well plates (96-well skirted pcr plate, 4ti-0740; 4titude, Wotton, UK) in a buffer that contained 150 mM NaCl, 20 mM HEPES pH 7.5, 1 mM CaCl$_2$, 0.5 mM TCEP, 0,01% Tween-20, and 50-nM fluorescent-labeled peptide (probe). The volume of the dilution series was 50 μL, which was later divided into three technical replicates of 15 μL during transferring to 384-well microplates (low binding microplate, 384 well, E18063G5; Greiner Bio-One, Kremsmünster, Austria). In total, the polarization of the probe was measured at eight different S100 concentrations (whereas one contains no S100 protein and corresponds to the free peptide). In competitive FP measurements, the same buffer was supplemented with S100 proteins to achieve a complex formation of 60–80%, based on the titration. Then, this mixture was used for creating a dilution series of the competitor (e.g., unlabeled peptide or purified protein) and the measurement was carried out identically as in the direct experiment. Competitive FP measurement was executed if the fitted K_d value originated from the direct FP titration was below 200 μM. Table 3 shows the peptides used for direct and competitive FP measurements. The typical experimental window of an S100 interaction was found to be around 100 mP (polarization). However, some direct titration caused marginally small change in the polarization signal (10–30 mP) that we decided not to analyze further.

Table 3. Peptides used in this study.

Name	Region	Sequence	Modification
fp53	p53 (17–56)	GSCETFSDLWKLLPENNVLSPLPSQAMD DLMLSPDDIEQWFTE	Fluorescein isothiocyanate
fRSK1	RSK1 (689–735)	GSCQDLQLVKGAMAATYSALNSSKPTPQL KPIESSILAQRRVRKLPSTTL	Fluorescein isothiocyanate
fNMIIA	NMIIA (1894–1937)	CRKLQRELEDATETADAMNREVSSLKNKL RRGDLPFVVPRRMARK	Fluorescein isothiocyanate
fMDM4	MDM4 (25–43)	NQVRPKLPLLKILHAAGAQ	N-terminal carboxyfluorescein
fCapZ	CapZ (265–276)	TRTKIDWNKILS	N-terminal carboxyfluorescein
fNCX1	NCX1 (254–265)	RRLLFYKYVYKR	N-terminal carboxyfluorescein
fTRPM4	TRPM4 (129–147)	VLQTWLQDLLRRGLVRAAQ	N-terminal carboxyfluorescein
fSIP	SIP (188–202)	SEGLMNVLKKIYEDG	N-terminal carboxyfluorescein
fC-ERMAD	C-ERMAD (516–560)	GSCKRITEAEKNERVQRQLLTLSSELSQAR DENKRTHNDIIHNENMRQG	Alexa Fluor 568 C5 maleimide
p53	p53 (1–60)	GSMEEPQSDPSVEPPLSQETFSDLWKLLPEN NVLSPLPSQAMDDLMLSPDDIEQWFTEDPGP	None (free N and C terminus)
NMIIA	NMIIA (1894–1937)	YRKLQRELEDATETADAMNREVSSLKNKLR RGDLPFVVPRRMARK	None (free N and C terminus)
MDM4	MDM4 (25–43)	NQVRPKLPLLKILHAAGAQ	None (free N and C terminus)
CapZ	CapZ (265–276)	TRTKIDWNKILS	None (free N and C terminus)
NCX1	NCX1 (254–265)	RRLLFYKYVYKR	None (free N and C terminus)
TRPM4	TRPM4 (129–147)	VLQTWLQDLLRRGLVRAAQ	None (free N and C terminus)
SIP	SIP (188–202)	SEGLMNVLKKIYEDG	None (free N and C terminus)
C-ERMAD	C-ERMAD (516–586)	GSCKRITEAEKNERVQRQLLTLSSELSQARD ENKRTHNDIIHNENMRQGRDKYKTLRQIRQ GNTKQRIDEFEAL	None (free N and C terminus)
FOR20	FOR20 (1–48)	GSMATVAELKAVLKDTLEKKGVLGHLKARIR AEVFNALDDDREPRPSLSH	None (free N and C terminus)
FOP	FOP (1–48)	GSYAATAAAVVAEEDTELRDLLVQTLENSGVL NRIKAELRAAVFLALEEQ	None (free N and C terminus)

Fitting of FP data

The K_d of the direct and competitive FP experiment was obtained by fitting the measured data with quadratic and competitive equation, respectively [7]. For automatic fitting, we used an in-house developed, Python-based program, called ProFit, which is freely available from GitHub. The program is capable to process multiple experimental data at once, evaluate direct competitive experimental data series pairs, and estimate the variance of the deduced parameters (e.g., dissociation constants) through a Monte Carlo approach. It produces ready-to-use figures for publications, as well as a report sheet for evaluation.

ITC measurements

Titrations were carried out either at 310 or at 298 K in a buffer containing 150 mM NaCl, 20 mM HEPES pH 7.5, 1 mM CaCl₂, 0.5 mM TCEP, using a MicroCal PEAQ-ITC instrument (Malvern Panalytical, Malvern, UK). The acquired data were fitted by PEAQ-ITC analysis software using the model 'One Set of Sites' for most of the experiments; however for S100B-CapZ and S100B-MDM4, this

model provided unsatisfactory fits and the model 'Two Sets of Sites' were applied instead. Note that we used the minimal interacting region (696–735) of RSK1 instead of the larger construct (689–735), which was used in the direct FP assay.

Bioinformatics analysis

For the phylogenetic analysis, the human S100 protein sequences were aligned using CLUSTALW [29] (gap open penalty 10 and gap extension penalty 0.1 for pairwise alignment; gap open penalty 10 and gap extension penalty 0.2 for multiple sequence alignment, BLOSUM weight matrix), MUSCLE [51], and PRANK [51] algorithms. Gaps were replaced by ambiguous residues (question marks) before the beginning and after the end of each sequence in the raw sequence alignment to avoid the overinterpretation of the highly variant tail extensions in the further analysis. Phylogeny was conducted with RAXML GUI [52]. Evolutionary history was inferred using maximum-likelihood algorithm with ProtGamma and LG as substitution model and substitution matrix, respectively [53], with 10 runs and 1000 bootstrap replicates. For the mapping of functional

relationships and clustering, the dendrogram from the S100ome data set was constructed using the unweighted pair-group method with arithmetic average (UPGMA) method [32] based on the Euclidean distance using the past software [54].

Acknowledgements

Conflict of interest

The authors declare no conflict of interest.

Author contributions

MAS carried out the experiments, analyzed the experimental data, and wrote the paper. GG and LN supervised the research, analyzed the data, and wrote the paper. PE, JK, GMK, ÁLP, and AR contributed by carrying out protein and peptide expression, ITC experiments, and bioinformatics analyses.

References

1 Zhou M, Li Q & Wang R (2016) Current experimental methods for characterizing protein-protein interactions. *ChemMedChem* **11**, 738–756.

2 Xing S, Wallmeroth N, Berendzen KW & Grefen C (2016) Techniques for the analysis of protein-protein interactions in vivo. *Plant Physiol* **171**, 727–758.

3 Brückner A, Polge C, Lentze N, Auerbach D & Schlattner U (2009) Yeast two-hybrid, a powerful tool for systems biology. *Int J Mol Sci* **10**, 2763–2788.

4 Goodson ML, Farboud B & Privalsky ML (2009) An improved high throughput protein-protein interaction assay for nuclear hormone receptors. *Nucl Recept Signal* **5**, e002.

5 Vincentelli R, Luck K, Poirson J, Polanowska J, Abdat J, Blémont M, Turchetto J, Iv F, Ricquier K, Straub ML *et al.* (2015) Quantifying domain-ligand affinities and specificities by high-throughput holdup assay. *Nat Methods* **12**, 787–793.

6 Hall MD, Yasgar A, Peryea T, Braisted JC, Jadhav A, Simeonov A & Coussens NP (2016) Fluorescence polarization assays in high-throughput screening and drug discovery: a review. *Methods Appl Fluoresc* **4**, 022001.

7 Roehrl MHA, Wang JY & Wagner G (2004) A general framework for development and data analysis of competitive high-throughput screens for small-molecule inhibitors of protein-protein interactions by fluorescence polarization. *Biochemistry* **43**, 16056–16066.

8 Roehrl MHA, Wang JY & Wagner G (2004) Discovery of small-molecule inhibitors of the NFAT-calcineurin interaction by competitive high-throughput fluorescence polarization screening. *Biochemistry* **43**, 16067–16075.

9 Donato R (1999) Functional roles of S100 proteins, calcium-binding proteins of the EF-hand type. *Biochim Biophys Acta* **1450**, 191–231.

10 Chen H, Xu C, Jin Q & Liu Z (2014) S100 protein family in human cancer. *Am J Cancer Res* **4**, 89–115.

11 Marenholz I, Heizmann CW & Fritz G (2004) S100 proteins in mouse and man: from evolution to function and pathology (including an update of the nomenclature). *Biochem Biophys Res Commun* **322**, 1111–1122.

12 Bresnick AR, Weber DJ & Zimmer DB (2015) S100 proteins in cancer. *Nat Rev Cancer* **15**, 96–109.

13 Bresnick AR (2018) S100 proteins as therapeutic targets. *Biophys Rev* **10**, 1617–1629.

14 Donato R (2001) S100: a multigenic family of calcium-modulated proteins of the EF-hand type with intracellular and extracellular functional roles. *Int J Biochem Cell Biol* **33**, 637–668.

15 Wheeler LC, Anderson JA, Morrison AJ, Wong CE & Harms MJ (2018) Conservation of specificity in two low-specificity proteins. *Biochemistry* **57**, 684–695.

16 Hartman KG, Vitolo MI, Pierce AD, Fox JM, Shapiro P, Martin SS, Wilder PT & Weber DJ (2014) Complex formation between s100b protein and the p90 ribosomal S6 kinase (RSK) in malignant melanoma is calcium-dependent and inhibits extracellular signal-regulated kinase (ERK)-mediated phosphorylation of RSK. *J Biol Chem* **289**, 12886–12895.

17 Inman KG, Yang R, Rustandi RR, Miller KE, Baldisseri DM & Weber DJ (2002) Solution NMR

structure of S100B bound to the high-affinity target peptide TRTK-12. *J Mol Biol* **324**, 1003–1014.

18 Kiss B, Duelli A, Radnai L, Kekesi KA, Katona G & Nyitray L (2012) Crystal structure of the S100A4-nonmuscle myosin IIA tail fragment complex reveals an asymmetric target binding mechanism. *Proc Natl Acad Sci USA* **109**, 6048–6053.

19 Biri-Kovács B, Kiss B, Vadászi H, Gógl G, Pálfy G, Török G, Homolya L, Bodor A & Nyitray L (2017) Ezrin interacts with S100A4 via both its N- and C-terminal domains. *PLoS ONE* **12**, e0177489.

20 Sakane K, Nishiguchi M, Denda M, Yamagchi F, Magari M, Kanayama N, Morishita R & Tokumitsu H (2017) Identification and characterization of a centrosomal protein, FOR20 as a novel S100A6 target. *Biochem Biophys Res Commun* **491**, 980–985.

21 Bousova K, Herman P, Vecer J, Bednarova L, Monincova L, Majer P, Vyklicky L, Vondrasek J & Teisinger J (2018) Shared CaM- and S100A1-binding epitopes in the distal TRPM4 N terminus. *FEBS J* **285**, 599–613.

22 van Dieck J, Fernandez-Fernandez MR, Veprintsev DB & Fersht AR (2009) Modulation of the oligomerization state of p53 by differential binding of proteins of the S100 family to p53 monomers and tetramers. *J Biol Chem* **284**, 13804–13811.

23 Wilder PT, Lin J, Bair CL, Charpentier TH, Yang D, Liriano M, Varney KM, Lee A, Oppenheim AB, Adhya S *et al.* (2006) Recognition of the tumor suppressor protein p53 and other protein targets by the calcium-binding protein S100B. *Biochim Biophys Acta* **1763**, 1284–1297.

24 Lin J, Blake M, Tang C, Zimmer D, Rustandi RR, Weber DJ & Carrier F (2002) Inhibition of p53 transcriptional activity by the S100B calcium-binding protein. *J Biol Chem* **276**, 35037–35041.

25 Rustandi RR, Baldisseri DM & Weber DJ (2000) Structure of the negative regulatory domain of p53 bound to S100B(ββ). *Nat Struct Biol* **7**, 570–574.

26 Lee Y-T, Dimotrova YN, Schneider G, Ridenour WB, Bhattacharya S, Soss SE, Caprioli RM, Filipek A & Chazin WJ (2008) Structure of the S100A6 complex with a fragment from the C-terminal domain of Siah-1 interacting protein: a novel mode for S100 protein target recognition. *Biochemistry* **47**, 10921–10932.

27 Gógl G, Alexa A, Kiss B, Katona G, Kovács M, Bodor A, Reményi A & Nyitray L (2015) Structural basis of ribosomal S6 kinase 1 (RSK1) inhibition by S100B protein. *J Biol Chem* **291**, 11–27.

28 Ecsédi P, Kiss B, Gógl G, Radnai L, Buday L, Koprivanacz K, Liliom K, Leveles I, Vértessy B, Jeszenői N *et al.* (2017) Regulation of the equilibrium between closed and open conformations of annexin A2 by N-terminal phosphorylation and S100A4-binding. *Structure* **25**, 1195–1207.

29 Zimmer DB, Eubanks JO, Ramakrishnan D & Criscitiello MF (2013) Evolution of the S100 family of calcium sensor proteins. *Cell Calcium* **53**, 170–179.

30 Wheeler LC, Donor MT, Prell JS & Harms MJ (2016) Multiple evolutionary origins of ubiquitous Cu2+ and Zn2+ binding in the s100 protein family. *PLoS ONE* **11**, e0164740.

31 Aguilar D, Aviles FX, Querol E & Sternberg MJE (2004) Analysis of phenetic trees based on metabolic capabilities across the three domains of life. *J Mol Biol* **340**, 491–512.

32 Sokal RR & Michener CD (1958) A statistical method for evaluating systematic relationships. *Univ Kansas Sci Bull* **38**, 1409–1438.

33 Gógl G, Biri-Kovács B, Durbesson F, Jane P, Nomine Y, Kostmann C, Bilics V, Simon M, Reményi A, Vincentelli R *et al.* (2019) Rewiring of RSK–PDZ interactome by linear motif phosphorylation. *J Mol Biol* **431**, 1234–1249.

34 Streicher WW, Lopez MM & Makhatadze GI (2010) Modulation of quaternary structure of S100 proteins by calcium ions. *Biophys Chem* **151**, 181–186.

35 Park S-H & Raines RT (2015) Fluorescence polarization assay to quantify protein-protein interactions. *Methods Mol Biol* **261**, 161–165.

36 Rossi AM & Taylor CW (2011) Analysis of protein-ligand interactions by fluorescence polarization. *Nat Protoc* **6**, 365–387.

37 Streicher WW, Lopez MM & Makhatadze GI (2009) Annexin I and annexin II N-terminal peptides binding to S100 protein family members: specificity and thermodynamic characterization. *Biochemistry* **48**, 2788–2798.

38 Wafer LN, Tzul FO, Pandharipande PP & Makhatadze GI (2013) Novel interactions of the TRTK12 peptide with S100 protein family members: specificity and thermodynamic characterization. *Biochemistry* **52**, 5844–5856.

39 Ecsédi P, Billington N, Pálfy G, Gógl G, Kiss B, Bulyáki É, Bodor A, Sellers JR & Nyitray XL (2018) Multiple S100 protein isoforms and C-terminal phosphorylation contribute to the paralog-selective regulation of nonmuscle myosin 2 filaments. *J Biol Chem* **293**, 14850–14867.

40 Shimamoto S, Kubota Y, Yamaguchi F, Tokumitsu H & Kobayashi R (2013) Ca 2+ /S100 proteins act as upstream regulators of the chaperone-associated ubiquitin ligase chip (c terminus of hsc70-interacting protein). *J Biol Chem* **288**, 7158–7168.

41 Shimamoto S, Kubota Y, Tokumitsu H & Kobayashi R (2010) S100 proteins regulate the interaction of Hsp90 with cyclophilin 40 and FKBP52 through their tetratricopeptide repeats. *FEBS Lett* **584**, 1119–1125.

42 Liu Y, Myrvang HK & Dekker LV (2015) Annexin A2 complexes with S100 proteins: structure, function and

pharmacological manipulation. *Br J Pharmacol* **172**, 1664–1676.

43 Fernandez-Fernandez MR, Rutherford TJ & Fersht AR (2008) Members of the S100 family bind p53 in two distinct ways. *Protein Sci* **17**, 1663–1670.

44 Schwaller B (2010) Cytosolic Ca2+ buffers. *Cold Spring Harb Perspect Biol* **2**, a004051.

45 Spratt DE, Barber KR, Marlatt NM, Ngo V, Macklin JA, Xiao Y, Konermann L, Duennwald ML & Shaw GS (2019) A subset of calcium-binding S100 proteins show preferential heterodimerization. *FEBS J* **286**, 1859–1876.

46 Wang S, Song R, Wang Z, Jing Z, Wang S & Ma J (2018) S100A8/A9 in inflammation. *Front Immunol* **9**, 1298.

47 Harms MJ & Thornton JW (2013) Evolutionary biochemistry: revealing the historical and physical causes of protein properties. *Nat Rev Genet* **14**, 559–571.

48 Kiss B, Ecsédi P, Simon M & Nyitray L (2019) Isolation and characterization of S100 protein-protein complexes. *Methods Mol Biol* **1929**, 325–338.

49 Anthis NJ & Clore GM (2013) Sequence-specific determination of protein and peptide concentrations by absorbance at 205 nm. *Protein Sci* **22**, 851–858.

50 Kuipers BJH & Gruppen H (2007) Prediction of molar extinction coefficients of proteins and peptides using UV absorption of the constituent amino acids at 214 nm to enable quantitative reverse phase high-performance liquid chromatography-mass spectrometry analysis. *J Agric Food Chem* **55**, 5445–5451.

51 Madeira F, Park YM, Lee J, Buso N, Gur T, Madhusoodanan N, Basutkar P, Tivey ARN, Potter SC, Finn RD *et al.* (2019) The EMBL-EBI search and sequence analysis tools APIs in 2019. *Nucleic Acids Res* **47**, W636–W641.

52 Silvestro D & Michalak I (2012) RaxmlGUI: a graphical front-end for RAxML. *Org Divers Evol* **12**, 335–337.

53 Le SQ & Gascuel O (2008) An improved general amino acid replacement matrix. *Mol Biol Evol* **25**, 1307–1320.

54 Hammer Ø, Harper DAT, Ryan PD, Ryan DD & Ryan PD (2011) PAST paleontological statistics. *Palaeontol Electron* **4**, 5–7.

Supporting information

Additional supporting information may be found online in the Supporting Information section at the end of the article.

Fig. S1. The interaction of the S100ome and p53 as measured by FP.

Fig. S2. The interaction of the S100ome and NMIIA as measured by FP.

Fig. S3. The interaction of the S100ome and CapZ (TRTK12) as measured by FP.

Fig. S4. The interaction of the S100ome and NCX1 as measured by FP.

Fig. S5. The interaction of the S100ome and C-ERMAD as measured by FP.

Fig. S6. The interaction of the S100ome and TRPM4 as measured by FP.

Fig. S7. The interaction of the S100ome and MDM4 as measured by FP.

Fig. S8. The interaction of the S100ome and SIP as measured by FP.

Fig. S9. The interaction of the S100ome and RSK1 as measured by FP.

Fig. S10. The interaction of the S100ome and MK2 as measured by FP.

Fig. S11. The interaction of the S100ome and MNK1 as measured by FP.

Fig. S12. The interaction of the S100ome and FOR20 as measured by FP.

Fig. S13. The interaction of the S100ome and FOP as measured by FP.

Fig. S14. The interaction of the labeled peptides and the unlabeled competitors.

Fig. S15. The selected S100 – peptide interactions measured by ITC.